www.elsevier.com/locate/sigpro

Image Detail Enhancement with Spatially Guided Filters

Shijie Hao, Daru Pan, Yanrong Guo, Richang Hong, Meng Wang

PII: S0165-1684(15)00083-3
DOI: http://dx.doi.org/10.1016/j.sigpro.2015.02.017
Reference: SIGPRO5741

To appear in: *Signal Processing*

Received date: 6 September 2014
Revised date: 20 February 2015
Accepted date: 21 February 2015

Cite this article as: Shijie Hao, Daru Pan, Yanrong Guo, Richang Hong, Meng Wang, Image Detail Enhancement with Spatially Guided Filters, *Signal Processing,* http://dx.doi.org/10.1016/j.sigpro.2015.02.017

Image Detail Enhancement with Spatially Guided Filters

Shijie Hao*[1, 2], Daru Pan[3], Yanrong Guo[4], Richang Hong[1], Meng Wang[1, 2]

1) School of Computer and Information, Hefei University of Technology, China

2) Computer Science and Technology Postdoctoral Research Station, Hefei University of Technology, China

3) School of Physics & Telecommunication Engineering, South China Normal University, China

4) Department of Radiology and BRIC, University of North Carolina at Chapel Hill, USA

Abstract: In recent years, enhancing image details without introducing artifacts has been attracting much attention in image processing community. Various image filtering methods have been proposed to achieve this goal. However, existing methods usually treat all pixels equally during the filtering process without considering the relationship between filtering strengths and image contents. In this paper, we address this issue by spatially distributing the filtering strengths with simple low-level features. First, to determine the pixel-wise filtering strength, we construct a spatially guided map, which exploits the spatial influence of image details based on the edge response of an image. Then, we further integrate this guided map into two state-of-the-art image filters and apply the improved filters to the task of image detail enhancement. Experiments demonstrate that our results generate better content-specific visual effects and introduce much less artifacts.

Keywords: Image detail enhancement, Spatially guided map, Guided image filter, Local Laplacian filter

*corresponding author; e-mail: hfut.hsj@gmail.com; telephone number: 86-13855147539

1 Introduction

With the rapid development of Internet technologies and photographing devices, we are witnessing the arrival of the multimedia era, which enables us to access plenty of photographic contents from all over the world. Many image processing methods, such as intelligent photographing [1, 2], content-based photo cropping [3, 4], detail manipulation [5, 6] and quality accessing [7, 8], are developed for better collecting and displaying images.

Among these applications, image detail manipulation is an important field, which keeps gaining attention in recent years. Pioneer works such as the anisotropic filter [9] and the bilateral filter [10] aim at smoothing image details while preserving the sharpness of salient edges. Recently, many other edge-aware filtering methods have been proposed [11-13] and their applications are also extended to detail enhancement, style transfer, haze removal, and so on. The key objective of these filters is to enhance or re-appear detail contents without introducing artifacts at a fine scale. However, these filters treat all pixels equally in terms of the filtering strength during the filtering process, which brings the following limitations. Due to the uniform filtering strength, on one hand, artifacts may be unnecessarily introduced along strong edges or in near-constant regions. On the other hand, these filters know little about how to distribute varying strengths to different regions. On the contrary, users may desire a content-specified effect according to its contents in many daily applications. For example, given a scenery image (Fig. 1(a)), one may prefer to enhance the details of the “rock” and “tree” regions while keep the naturalness of the “sky” and “cloud”

regions. To this end, a spatially guided map that approximates regions of these contents can be developed to control the pixel-wise filtering process. However, given the existence of the semantic gap between low-level features and high-level contents, it remains a challenging task to accurately delineate the boundaries between different semantic regions. To bridge this gap, recent learning based methods [14-17] have been proposed to add semantic tags in images. However, the annotations are usually not detailed at the pixel level.

In this paper, instead of specifying concrete labels of image regions, we construct a spatially guided map, which approximates the spatial influences based on simple edge features. Then we integrate the obtained map into two state-of-the-art filtering models and apply both improved models in the task of image detail enhancement. Our model is characteristic in the following aspects. First, the guided map forms a generally accurate approximation on the distribution and intensity of image details (e.g. Fig. 1 (c)), which allows a detail-specific filtering process. Second, the filtering result based on our method generates more natural effects and introduces less artifacts such as edge halos, over-exaggerated details and noises in the meanwhile (e.g. Fig. 1 (b, d)). Third, our model only relies on simple low-level features and thus has low computational costs.

The rest of this paper is organized as follows. Section 2 briefly introduces the related works. We propose our spatially guided map in Section 3 and present its combination with two existing filtering models in Section 4. Experiments for

validating the effectiveness of our method are demonstrated in Section 5. Finally, Section 6 concludes the paper and discusses possible future works.

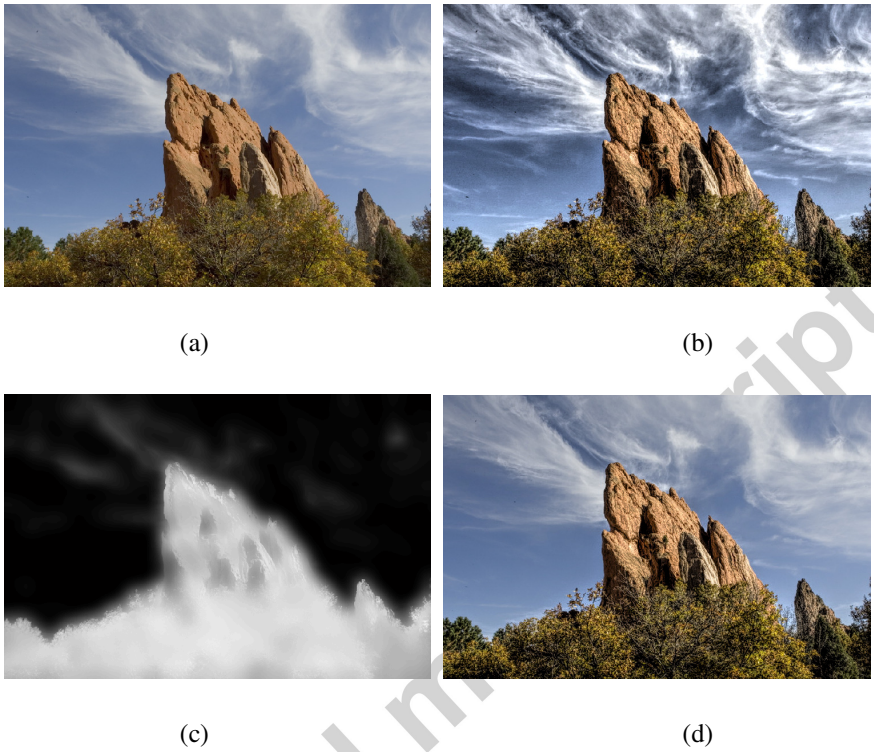

(a) (b)

(c) (d)

Fig. 1 An example of enhancing the input image (a) with a uniform filtering strength (b) and with dynamically filtering strengths (d) based on the spatially guided map (c)

2 Related Works

To overcome the blurring limitation of traditional average filters such as the mean and Gaussian filter [18], weighted average filters were proposed to generate the edge-preserving effects. For example, the anisotropic filter [9] uses the gradient information to guide the diffusion process. The bilateral filter [10] averages neighboring pixels according to the weights determined by Gaussian functions of both intensity and spatial distance. After that, this model was extended to the joint bilateral filter [19], which determines the weights by introducing an extra image with a

different light condition. He et al. [13] further generalized the bilateral filter to the guided image filter. This method transfers the structure of the guidance image to the filtering output, and is successfully applied in tasks such as image matting, haze removal and super-resolution.

As another trend of methods in edge-aware image processing, details can be manipulated at multiple scales. These methods often involve solving a global optimization problem [5, 6, 20, 21], which could be limited in its scalability. Differently, Paris et al. [22] proposed the local Laplacian filter (LLF) by linearly processing and combing Gaussian and Laplacian image pyramids, which used to be considered as inappropriate for generating edge-preserving results. However, this filter is computationally expensive to some extent. To relieve this limitation, Aubry et al. [23] proposed a fast LLF algorithm with O(N) complexity (N is the number of pixels of an image) based on the signal processing theory. They also pointed out the relationships between the LLF and bilateral filter, i.e. the LLF with two-level Gaussian and Laplacian pyramids is essentially an unnormalized bilateral filter.

However, the above-mentioned methods do not consider a spatial distribution of image contents, which can be different with respect to the detail richness. Addressing this problem, Hao et al. [24] proposed an improved LLF by introducing a spatial guidance map based on the distance transform (DT) function. The proposed method in this paper is different from [24] in twofold. First, the distance transform function tends to generate block effects. And the spatial guidance map based on the distance transform function poorly distinguishes the boundaries between regions of image

contents. Differently, we propose a novel and generalized scheme on constructing the guidance map. Second, our model can be applied to approaches more than LLF, which also achieves satisfying results. The similar idea of exploiting spatial information has also been employed in fields like multimedia and computer vision. In [25], the system detects less detailed regions within each frame and dynamically places video captions. Visual attention models [26-28] can be also considered as the process of computing a map of spatial importance of image contents to some extent. Besides, Tang et al. [7] designed a content-based image quality assessment framework, which is composed of three steps, i.e. category classifying, subject segmentation and human perception modeling, by leveraging multiple features (from low-level to high-level).

3 Spatially Guided Map

In this section, we construct the spatially guided map $\boldsymbol{S}$ of an image $\boldsymbol{I}$, which is essentially a scalar matrix of the same size as the image, to quantify the spatial influence of image details based on simple edge features of $\boldsymbol{I}$. The flowchart is shown in Fig. 2. The details of this process are described as follows.

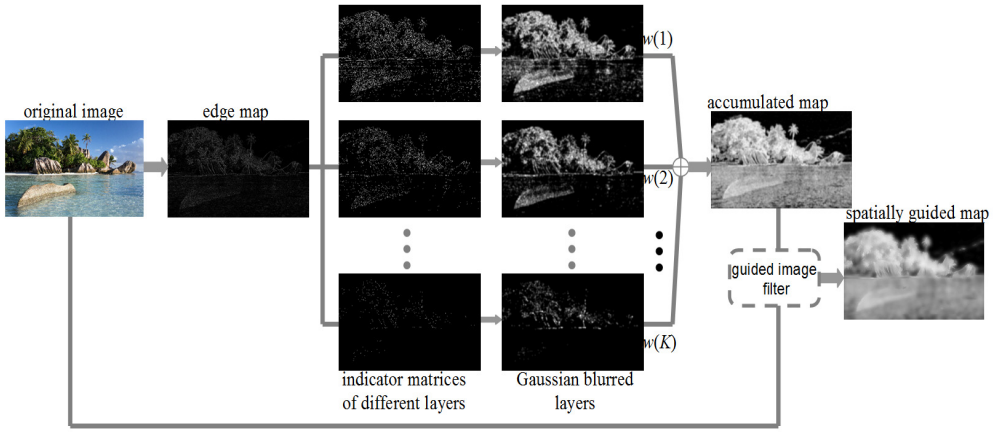

Fig. 2 The flowchart of building our spatially guided map

Given the edge response $|\nabla \boldsymbol{I}|$ of the image $\boldsymbol{I}$ on the domain Ω, we define a spatial indicator function $f(i)$ at $(x,y)\in\Omega$:

$$f_{(x,y)}(i)=\begin{cases}1, & \text{if } |\nabla \boldsymbol{I}(x,y)|=i\\ 0, & \text{else}\end{cases} \tag{1}$$

where i is the normalized intensity in the edge response. By collecting all the $f_{(x,y)}(i)$s in Ω, we can obtain an indicator matrix $\boldsymbol{f}_{\Omega}(i)$, which carries the spatial information of image details at one isolated layer with respect to i. We then formulate the spatial influence of the details by a Gaussian diffusion process through the Gaussian convolution. By integrating all the convoluted matrices of all the layers, an accumulated map can be obtained as follows:

$$\boldsymbol{S}_a^{'}=\int_0^1 \boldsymbol{f}_{\Omega}(i)*G(r)\ \ \mathrm{d}i \tag{2}$$

In Eq. 2, the produced map assigns the equal weight to all the layers (intensities), which is limited in emphasizing higher (thus possibly important) edge responses. So we choose a weight function, i.e. $w(i)=1-h(i)$, where $h(i)$ is the statistical distribution with respect to i and can be easily estimated by the histogram of $|\nabla \boldsymbol{I}|$. Therefore, the accumulated map is thereof improved as

$$\boldsymbol{S}_a=\int_0^1 \boldsymbol{f}_{\Omega}(i)*G(r)w(i)\ \ \mathrm{d}i \tag{3}$$

The inverse-histogram $1-h(i)$ is chosen as the weight function mainly due to the following observations. On one hand, in most cases, strong edges tend to have large impacts on forming the main image structures and thus they are more likely to attract the human attention. However, their proportion in the edge response is often relatively small. On the other hand, weak edges, which can be subtle structures or even noisy fluctuations, constitute an overwhelming proportion of the edge map. In this situation,

compared with using equal weights as in [24], the adaptive weight function can better address this imbalance by boosting strong edges while ignoring tiny variations.

As a further step, we refine the accumulated map $\boldsymbol{S}_a$ by adopting the guided image filter. This produces the final spatially guided map, i.e. $\boldsymbol{S}$, for the task of image detail enhancement. In the filtering process, we employ the original image $\boldsymbol{I}$ at hand as the guidance image, which leverages the self-complementary information of the original image. As is shown in Fig. 3, the benefits of this step are explained as follows. First, compared with $\boldsymbol{S}_a$, $\boldsymbol{S}$ has a more faithful piece-wise approximation on the detail density since the model of guided image filter in [13] assumes a linear dependency between the output and guidance image. Second, $\boldsymbol{S}$ generates smoothly varied regions along strong edges, which effectively avoids artifacts.

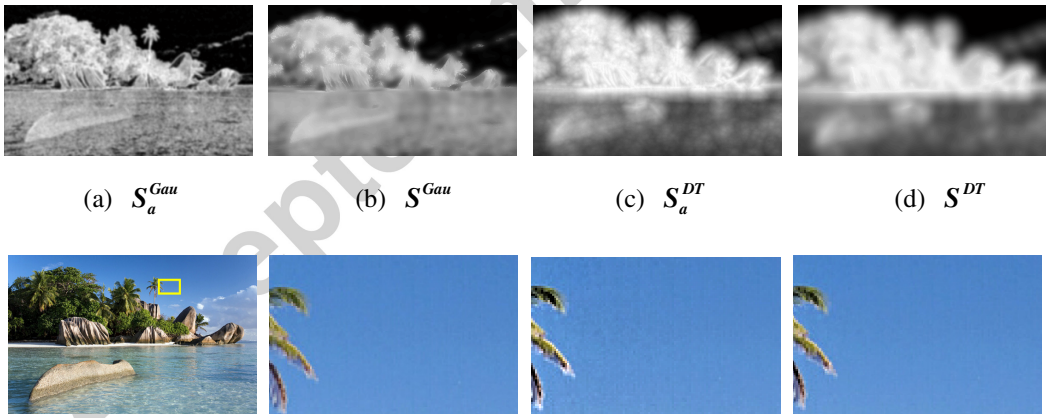

(a) $\boldsymbol{S}_a^{Gau}$ (b) $\boldsymbol{S}^{Gau}$ (c) $\boldsymbol{S}_a^{DT}$ (d) $\boldsymbol{S}^{DT}$

(e) original image (f) enlarged view (g) result based on $\boldsymbol{S}^{DT}$ (h) result based on $\boldsymbol{S}^{Gau}$

Fig. 3 Comparisons of different spatial guided maps $\boldsymbol{S}_a^{DT}$ and $\boldsymbol{S}^{DT}$ are based on the distance transform function [24] while $\boldsymbol{S}_a^{Gau}$ and $\boldsymbol{S}^{Gau}$ are based on the Gaussian kernel.

We also compare the spatially guided maps based on the DT function ($\boldsymbol{S}_a^{DT}$ and $\boldsymbol{S}^{DT}$) and the Gaussian kernel ($\boldsymbol{S}_a^{Gau}$ and $\boldsymbol{S}^{Gau}$) in Fig. 3. As for the DT based guiding map, the DT function is more diffused in the geometric morphology while the Gaussian kernel has much better flexibility at a small controlling parameter σ. Therefore, we can empirically see from Fig. 3 that the DT based map used in [24] has limited performance along the borderlines in terms of discriminating power, which generates obvious inconsistent filtering output in plain regions, such as the enlarged sky region in Fig. 3(g).

Following gives the computational cost analysis for our method. The complexity of computing accumulated map is linear with the image pixels. Its computation cost mainly stems from the Gaussian convolution and the integral discretization in Eq. 3. With the Gaussian blur width σ and the number of discretized layers K, the complexity is $\mathrm{O}(K \cdot \sigma^2 N)$ in brute force, where N is the number of pixels of an image. Aiming at further acceleration, the Gaussian blur is approximated as n iterations of the $\mathrm{O}(N)$ box filtering, which is independent of the kernel size. We empirically find that the experimental results based on this approximation with a very small n are approximately identical with the results based on the brute force implementation.

4 Detail Enhancement Based on the Spatially Guided Map

In this section, we improve the guided image filter [13] and the LLF [23] by integrating our spatially guided map model respectively, and then apply both improved models in the task of image detail enhancement.

4.1 Spatially Guided Image Filter

Given the input image $\boldsymbol{I}$ and a guide image $\boldsymbol{I}_{\mathrm{g}}$, the model of guided image filtering assumes a linear dependency between its output $\boldsymbol{I}_{\mathrm{o}}$ and $\boldsymbol{I}_{g}$:

$$\boldsymbol{I}_{\mathrm{o}}(x,y) = a_k \boldsymbol{I}_{\mathrm{g}}(x,y) + b_k, \quad \forall (x,y) \in \Omega_k \tag{4}$$

where Ω_k is an image patch centered at the pixel *k*. According to the linear ridge regression technique, the coefficients a_k and b_k are estimated as

$$a_k = \frac{|\Omega_k|^{-1} \sum_{(x,y)\in\Omega_k} \boldsymbol{I}_{\mathrm{g}}(x,y)\boldsymbol{I}(x,y) - \mu_k \bar{I}_k}{\sigma_k^2 + \varepsilon} \tag{5}$$

$$b_k = \bar{I}_k - a_k \mu_k \tag{6}$$

where μ_k and σ_k^2 are the mean and variance of $\boldsymbol{I}_{\mathrm{g}}$ in Ω_k, $\bar{I}_k$ is the mean of $\boldsymbol{I}$ in Ω_k, and ε is the regularization parameter used in the regression.

In detail enhancement, $\boldsymbol{I}$ and $\boldsymbol{I}_{\mathrm{g}}$ are identically selected as the original input image. From the view of signal processing, the $\boldsymbol{I}_{\mathrm{o}}$ is thereof the base layer $\boldsymbol{I}_{\mathrm{b}}$, which reflects the basic image contents at low frequencies, while $\boldsymbol{I}_r = \boldsymbol{I} - \boldsymbol{I}_{\mathrm{o}}$ is the residual layer which reflects image details at high frequencies. Therefore the detail enhancing model can be simply constructed as a linear combination of $\boldsymbol{I}_{\mathrm{b}}$ and $\boldsymbol{I}_r$:

$$\boldsymbol{I} = \boldsymbol{I}_{\mathrm{b}} + S_0 \cdot \boldsymbol{I}_r \tag{7}$$

where S_0 is the scalar filtering strength. We extend this model into the spatially guided image filtering by introducing the spatially guidance map $\boldsymbol{S}$ proposed in Section 3:

$$\boldsymbol{I}(x,y) = \boldsymbol{I}_{\mathrm{b}}(x,y) + S_0 \cdot \boldsymbol{S}(x,y) \cdot \boldsymbol{I}_r(x,y) \quad \forall (x,y) \in \Omega \tag{8}$$

In this way, each pixel is equipped with its own filtering strength distributed by the spatially guided map. As for the computational cost, the improved guide image filter

remains at $O(\mathrm{C}_1 N)$ where C_1 is a constant.

Here it needs to be noted that, on the premise that the input and guide image are homologous and share the same size, the choice of the input is task-specific. In Section 3, we have applied the guided image filter to refine the accumulated map, where $\boldsymbol{S}_a$ is taken as the input image while the guided image is still the original $\boldsymbol{I}$. Due to the constructed linear dependency (Eq. 4), the structure of $\boldsymbol{I}$ is smoothly transferred to the raw spatial map $\boldsymbol{S}_a$. This post-processing yields the much refined output, i.e. the final $\boldsymbol{S}$, which resembles the idea of refining the raw transmission map in the application of single haze removal as mentioned in [13].

4.2 Spatially Guided LLF

Different from the guided image filter, the LLF manipulates an image at multiple scales $l = \{1, ..., L\}$ with the Gaussian pyramid $\{\boldsymbol{G}_l\}$ and Laplacian pyramid $\{\boldsymbol{L}_l\}$ of the input image. In principle, by defining a remap function $r(i)$, the LLF remaps the values of all pixels in $\{\boldsymbol{L}_l\}$ based on $r(i)$ and reconstructs the output image at the finest scale by collapsing the $\{\boldsymbol{L}_l\}$. Aiming at speeding up this process, Aubry et al. [24] pre-compute a few remapped Laplacian pyramids at a fraction of values evenly sampled from the normalized intensity range [0, 1], and then reconstruct the remapped pyramids of the rest values with a linear interpolation. This approximation reduces the complexity to $O(\mathrm{C}_2 N)$ in which C_2 is also a constant.

As for the remapping function for detail enhancement, a Gaussian shape mapping is modeled as follows:

$$r(i) = i + S_0 \cdot (i - g) \cdot \exp((i - g)^2 / 2\delta^2) \tag{9}$$

where i and g are both normalized intensities, and δ is the ranging parameter. Fig. 4 gives some typical examples of $r(i)$. It can be observed that, compared to a smaller S_0 (e.g. $S_0 = 1$), a bigger S_0 (e.g. $S_0 = 5$) remaps the small interval into a large one, which implies an amplification of image details. Therefore S_0 is able to represent the scalar filtering strength similarly in Eq. 7. Based on the spatially guided map $\boldsymbol{S}$, we can also extend the conventional remapping function into:

$$r_{(x,y)}(i) = i + S_0 \cdot \boldsymbol{S}(x,y) \cdot (i-g) \cdot \exp((i-g)^2 / 2\delta^2) \tag{10}$$

In this way, we can construct the the spatially guided LLF, which dynamically distributes the filtering strengths to all the pixels in $\boldsymbol{I}$. It should also be noted that the complexity of the improved LLF remains at the same level with the original fast LLF.

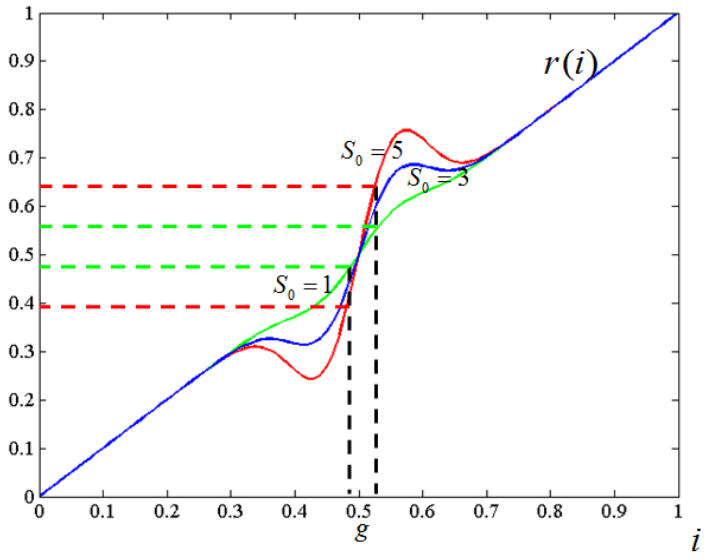

Fig. 4 Remapping functions $r(i)$ centered at g with different strengths

5 Experimental Results

In this section, we demonstrate the effectiveness of the proposed spatially guided image filter and spatially guided LLF in the application of image detail enhancing. The algorithms are all implemented with MATALB codes in a single thread at a laptop

with 2.6GHz CPU and 4G ROM. For all the experiments, the parameters settings are as follows. For computing $\boldsymbol{S}_a$ based on Eq.3, we choose K=16 and $\sigma = 0.02 \cdot \min(\text{width}, \text{height})$. As for the guided image filter for extracting the base layer $\boldsymbol{I}_{\text{b}}$ and refining the accumulated map $\boldsymbol{S}_a$, we consistently choose the size of Ω_k as σ and we set ε as 0.01. In LLF, δ is set to 1/16 and the number of pre-computed image pyramids is chosen as 16.

(a) input image (b) accumulated map $\boldsymbol{S}_a$ (c) spatially guided map $\boldsymbol{S}$

(d.1) mild enhancing (d.2) median enhancing (d.3) strong enhancing

(d) spatially guided image filter

(e.1) mild enhancing (e.2) median enhancing (e.3) strong enhancing

(e) spatially guided LLF

Fig. 5 Enhancing results with different $S_0 s$ respectively based on spatially guided image filter (the second row) and spatially LLF (the third row)

The key parameter to control the overall filtering strength is S_0, which is actually a

multiplier factor of the spatially guided map. As is shown in Fig. 5, we gradually increase S_0 to obtain different effects at progressive strengths based on the two improved methods (i.e. Fig. 5(d, e)). In general, we observe that our method generates content-specific enhancing results under different $S_0 s$. The building with rich textures is gradually amplified with the increasing of S_0, while plain regions like the sky consistently remain the same. This visual effect benefits from the non-uniform filtering strengths determined in the map $\boldsymbol{S}$, which roughly estimates distribution of image content details in terms of their positions and intensities. As for the computational costs, it respectively takes about 0.9 second and 0.4 second to compute $\boldsymbol{S}$ and $\boldsymbol{I}_{\mathrm{b}}$ in the spatially guided image filtering. In the spatially guided LLF, it takes 1.3 second in the remapping process with the Laplacian pyramid $\{\boldsymbol{L}_l\}$.

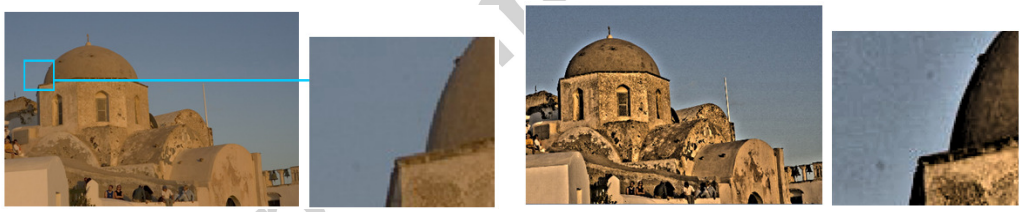

(a) input image (b) the result with uniform filtering strength

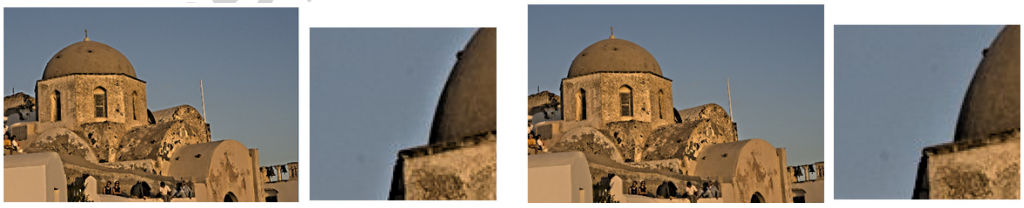

(c) the result with accumulated map $\boldsymbol{S}_a$ (d) the result with spatially guided map $\boldsymbol{S}$

Fig. 6 Comparison of results based on the original image guided filter [13], and its improved versions based on spatially guided maps. The $S_0 s$ in three methods are the same.

(a) input image (b) the result with uniform filtering strength

(c) the result with accumulated map $\boldsymbol{S}_a$ (d) the result with spatially guided map $\boldsymbol{S}$

Fig. 7 Comparison of results based on original fast LLF [23], and its improved versions based on spatially guided maps. The result in (c) is based on the intermediate accumulated map $\boldsymbol{S}_a$ and the result in (d) is based on the final spatially guided map $\boldsymbol{S}$. The $S_0 s$ in three methods are the same.

We further compare the results based on the spatially guided map $\boldsymbol{S}$, the accumulated map $\boldsymbol{S}_a$ and the uniform mapping. i.e. the original guided image filter

and LLF. As is shown in Fig. 6, the result of the original filter (Fig. 6(b)) over-exaggerates the tiny variations in the whole sky region and produces clear halos along the borderlines of strong edges, which makes the output image visually unnatural to some extent. In contrary, spatially guided results (Fig. 6(c and d)) generally overcome these limitations. Specifically, by comparing those enlarged views, the result based on the refined map $\boldsymbol{S}$ (Fig. 6(d)) outperforms its counterpart based on $\boldsymbol{S}_a$ (Fig. 6(c)) in terms of introducing much less halos along the backbone edge between the building and sky region. As for the LLF based methods, the experimental results in Fig. 7 also demonstrate the benefits of the proposed spatially guided map. Due to the inherited halo-free characteristic of LLF, all three results based on uniform mapping (Fig. 7(b)), $\boldsymbol{S}_a$ (Fig. 7(c)) and $\boldsymbol{S}$ (Fig. 7(d)) generate little gradient reversal effects (as shown in the left enlarged region). Moreover, compared with $\boldsymbol{S}_a$, the refined map $\boldsymbol{S}$ has better performance in suppressing the turbulence of near the pole (the right enlarged region) in the input image. It is due to the fact that $\boldsymbol{S}$ has a more smoothed variation along the edge borderlines, which is experimentally validated in the first row of Fig. 5.

6 Conclusions

In this paper, we propose the spatially guided map based on the simple edge response of an image. We further integrate this map into the guided image filter and the local Laplacian filter to dynamically impose the filtering strengths for enhancing image details. Experimental results show better performances of our method in terms of enhancing image details while keeping its naturalness. From the above-mentioned

sections, we can observe that the process of constructing the spatially guided map is independent of the type of image filters and enhancing models. So the map can be easily integrated into other filters, e.g. the family of bilateral filtering methods.

We plan to further our research in the following aspects. First, since our improved model performs a pixel-wise filtering style, parallel techniques could be considered to further speed up the algorithms in real applications. Second, we can follow a few novel ideas to extend our research. For example, instead of local low-level features, we would leverage multiple features in learning schemes [29-31] to detect object regions at the semantic level. Also, we can adopt some representative techniques [32-34] to learn and quantitatively evaluate the aesthetics of the our results.

Acknowledgments: The authors sincerely appreciate the useful comments and suggestions from the anonymous reviewers. This work was supported by National Natural Science Fund of China (Grant No. 61301222), China Postdoctoral Science Foundation (Grant No. 2013M541821), Fundamental Research Funds for the Central Universities (Grant No. 2013HGQC0018, 2013HGBH0027, 2013HGBZ0166)

Reference

[1] B. Ni, M. Xu, B. Cheng, M. Wang, S. Yan, Q. Tian. Learning to photograph: a compositional perspective. IEEE Transactions on Multimedia, 15(5): 1138-1151, 2013

[2] W. Yin, T. Mei, C. Chen. Socialized mobile photography: learning to photograph with social context via mobile devices. IEEE Transactions on Multimedia, 16(1): 184-200, 2014

[3] L. Zhang, M.Song, Y. Yang, Q. Zhao, C. Zhao, N.Sebe. Weakly Supervised Photo Cropping.

IEEE Transactions on Multimedia, 16(1): 94-107, 2014

[4] L. Zhang, M. Song, Q. Zhao, X. Liu, J. Bu, C. Chen. Probabilistic Graphlet Transfer for Photo Cropping. IEEE Transactions on Image Processing, 22(2): 802-815, 2013

[5] Z. Farbman, R. Fattal, D. Lischinski, R. Szeliski. Edge-preserving decompositions for multi-scale tone and detail manipulation. ACM Transactions on Graphics (SIGGRAPH 2008), 27(3): article 67

[6] X. Li, Y. Gu, S. Hu, R. Martin. Mixed-Domain Edge-Aware Image Manipulation. IEEE Transactions on Image Processing, 22(5): 1915-1925, 2013

[7] X. Tang, W. Luo, X. Wang. Content-Based Photo Quality Assessment. IEEE Transactions on Multimedia, 15(8): 1930-1943, 2013

[8] Z. Wang, A.C. Bovik, H.R. Sheikh and E.P. Simoncelli. Image quality assessment: from error visibility to structural similarity. IEEE Transactions on Image Processing, 13(4): 600-612, 2004

[9] P. Perona, J. Malik. Scale-space and edge detection using anisotropic diffusion. IEEE Transactions on Pattern Analysis and Machine Intelligence, 12(7): 629–639, 1990

[10] C. Tomasi, R. Manduchi. Bilateral filtering for gray and color images. In Proceedings of ICCV, 1998

[11] R. Fattal. Edge-avoiding wavelets and their applications. ACM Transactions on Graphics, 28(3): Article 22, 2009

[12] S. Paris, S. W. Hasinoff, J. Kautz. Local Laplacian filters: edge-aware image processing with a Laplacian pyramid," ACM Transactions on Graphics, 30(4): Article 68, 2011

[13] K. He, J Sun, X. Tang. Guided image fitler. IEEE Transactions on Pattern Analysis and Machine Intelligence, 35(6): 1397-1409, 2013

[14] M. Wang, B. Ni, X. Hua, T.Chua. Assistive tagging: A survey of multimedia tagging with human-computer joint exploration. ACM Computing Surveys, 44(4): Article 25, 2012

[15] R. Hong, M. Wang, Y. Gao, D. Tao, X. Li, X. Wu. Image Annotation by Multiple-Instance Learning With Discriminative Feature Mapping and Selection. IEEE Transactions on Cybernetics, 44(5): 669-680, 2014

[16] M. Wang, X. Hua, R. Hong, J. Tang, G. Qi, Y. Song. Unified Video Annotation via Multigraph Learning. IEEE Transactions on Circuits and Systems for Video Technology, 19(5): 733-746, 2009

[17] Y. Gao, M. Wang, Z. Zha, J. Shen, X. Li, X. Wu. Visual-Textual Joint Relevance Learning for Tag-Based Social Image Search. IEEE Transactions on Image Processing 22(1): 363-376, 2013

[18] R. Gonzalez, R. Woods. Digital Image Processing, second edition Prentice Hall, 2002.

[19] G. Petschnigg, M. Agrawala, H. Hoppe, R. Szeliski, M. Cohen, K. Toyama. Digital Photography with Flash and No-Flash Image Pairs. ACM Transactions on Graphics (SIGGRAPH 2004), 23(3): 664-672

[20] L. Xu, C. Lu, Y. Xu, J. Jia. Image smoothing via L0 gradient minimization. ACM Transactions on Graphics (SIGGRAPH Asia 2011), 30(6): Article 174

[21] K. Subr, C. Soler, F. Durand. Edge-preserving multiscale image decomposition based on local extrema. ACM Transactions on Graphics (SIGGRAPH Asia 2009).28(5): Article 147

[22] S. Paris, S. Hasinoff, J. Kautz. Local Laplacian filters: edge-aware image processing with a Laplacian pyramid. ACM Transactions on Graphics (SIGGRAPH 2011), 30(4): article 68

[23] M. Aubry, S. Paris, S. Hasinoff, J. Kautz, F. Durand. Fast local Laplacian Filters: theory and applications. In Proceedings of ACM SIGGRAPH, 2014

[24] S. Hao, M. Wang, R. Hong, J. Jiang. Spatially guided local Laplacian filter for nature image

detail enhancement. Multimedia Tools and Applications. In press.

[25] R. Hong, M. Wang, M. Xu, S. Yan, T. Chua. Dynamic captioning: video accessibility enhancement for hearing impairment. In Proceedins of ACM Multimedia, 2010

[26] P. Rosin. A simple method for detecting salient regions. Pattern Recognition, 42(11): 2363-2371, 2009

[27] L. Zhang, Y. Xia, R. Ji, X. Li. Spatial-Aware Object-Level Saliency Prediction by Learning Graphlet Hierarchies. IEEE Transactions on Industrial Electronics, 62(2): 1301-1308, 2015

[28] M. Cheng, G. Zhang, N. Mitra, X. Huang, S. Hu. Global Contrast based Salient Region Detection. In Proceedings of CVPR, 2011

[29] M. Wang, X. Hua. Active learning in multimedia annotation and retrieval: A survey. ACM Transactions on Intelligent Systems and Technology, 2(2): Article 10, 2011

[30] L. Zhang, Y. Gao, Y. Xia, K Lu, J. Shen, R. Ji. Representative Discovery of Structure Cues for Weakly-Supervised Image Segmentation. IEEE Transactions on Multimedia, 16(2): 470-479, 2014

[31] A. Kapoor, J. Caicedo, D. Lischinski, S. Kang. Collaborative Personalization of Image Enhancement. International Journal of Computer Vision, 108:148-164, 2014

[32] S. Bhattacharya, R. Sukthankar, M. Shah. A framework for photo-quality assessment and enhancement based on visual aesthetics. In Preceedings of ACM Multimedia, 2010

[33] L. Zhang, Y. Gao, R.Zimmermann, Q. Tian, X. Li. Fusion of Multichannel Local and Global Structural Cues for Photo Aesthetics Evaluation. IEEE Transactions on Image Processing, 23(3): 1419-1420, 2014

[34] L. Marchesotti, F. Perronnin, D. Larlus, G. Csurka. Assessing the aesthetic quality of photographs using generic image descriptors.In Proceedings of the International Conference on Computer Vision (ICCV), 2011

Research highlights:

We construct a spatially guided map exploiting spatial influences of edge features.

We improve two state-of-the-art filters by integrating our spatially guided map.

Better filtering results are obtained with more naturalness and less artifacts.